Composition dependence of vesicle morphology and mixing properties in a bacterial model membrane system

B. Pozo Navas[a], K. Lohner[a,*], G. Deutsch[a], E. Sevcsik[a], K.A. Riske[b], R. Dimova[b], P. Garidel[c], G. Pabst[a]

[a]Institute of Biophysics and X-ray Structure Research, Austrian Academy of Sciences, Schmiedlstraße 6, A-8042 Graz, Austria
[b]Max Planck Institute of Colloids and Interfaces, Theory Department, Am Mühlenberg 1, D-14476 Golm, Germany
[c]Martin-Luther-University Halle/Wittenberg, Institute of Physical Chemistry, Mühlpforte 1, D-06108 Halle/Saale, Germany

Abstract

We have determined the mixing properties and lamellar organization of bacterial membrane mimetics composed of 1-palmitoyl-2-oleoyl-phosphatidylethanolamine (POPE) and -phosphatidylglycerol (POPG) at various molar ratios applying differential scanning calorimetry, small and wide-angle X-ray scattering, as well as optical phase contrast microscopy. Combining the experimental thermodynamic data with a simulation of the liquidus and solidus lines, we were able to construct a phase diagram. Using this approach, we find that the lipids mix in all phases non-ideally in the thermodynamic sense. As expected, pure POPE assembles into multilamellar and pure POPG into unilamellar vesicles, respectively, which are stable within the studied temperature range. In contrast, mixtures of the two components form oligolamellar vesicles consisting of about three to five bilayers. The layers within these oligolamellar liposomes are positionally correlated within the gel phase, but become uncorrelated within the fluid phase exhibiting freely fluctuating bilayers, while the vesicles as a whole remain intact and do not break up into unilamellar forms. X-ray, as well as DSC data, respectively, reveal a miscibility gap due to a lateral phase segregation at POPG concentrations above about 70 mol%, similar to previously reported data on mixtures composed of disaturated PEs and PGs. Hence, the existence of a region of immiscibility is a general feature of PE/PG mixtures and the mixing properties are dominated by PE/PG headgroup interactions, but are largely independent of the composition of the hydrocarbon chains. This is in accordance with a recent theoretical prediction.
© 2005 Elsevier B.V. All rights reserved.

1. Introduction

Biological membranes are complex systems which have attracted scientific interest for a long time and for various reasons. Recently, research has focused on bacterial membranes because several antimicrobial peptides were found to destabilize and destroy only bacteria but leave mammalian cells unaffected [1–3]. This feature is the key to the rational development of new antibiotic drugs to fight infectious diseases [3]. Besides the present lack of an unambiguous understanding of the mechanisms of anti-microbial peptide action, it is evident that the bacterial membrane poses a barrier–and therefore essential site of interaction–that needs to be either overcome or destroyed [4]. One of the major reasons that allow antimicrobial peptides to discriminate between bacterial and mammalian cells is thought to be due to their different lipid composition and physical properties [3].

Mammalian cytoplasmic membranes contain mainly phosphatidylcholine (PC), sphingomyelin, phosphatidylser-ine, phosphatidylethanolamine (PE) and cholesterol [5]. The phospholipids are asymmetrically distributed between the outer and the inner lipid leaflet, with PC and sphingomyelin being enriched in the outer monolayer [6]. Bacterial

* Corresponding author. Tel.: +43 316 4120 323; fax: +43 316 4120 390.
E-mail address: Karl.Lohner@oeaw.ac.at (K. Lohner).

membranes, on the other hand, contain to a large extend PE and phosphatidylglycerol (PG), or PG derivatives such as diphosphatidylglycerol (DPG) or cardiolipin, but lack cholesterol ([3], and references therein). Further, the lipid composition depends also on whether the bacterium belongs to the class of Gram-negative or Gram-positive bacteria [7,8]. In general, higher amounts of PEs are found in the inner membrane of Gram-negative bacteria, while cytoplasmic membranes of Gram-positive bacteria are richer in PG content. For example, PE represents about 82 wt.% of the inner cytoplasmic membrane of *Escherichia coli*, whereas PG and its derivatives are the predominant phospholipid components of the *Staphylococcus aureus* membrane. Qualitatively, it is apparent that different lipid compositions alter global membrane properties, such as structure, packing density, bending rigidity, surface charge density, to name but a few. In order to gain some quantitative insight, it is convenient to study model membranes composed of phospholipids only [9]. In the present case, our aim is to elucidate the properties of bacterial model membranes by studying binary mixtures of PE and PG under physiologically relevant buffer conditions (20 mM Na-phosphate buffer, pH 7.4, 130 mM NaCl).

The two lipids exhibit several different properties. PEs are zwitterionic amphiphiles and self assemble, in the presence of an aqueous solution, into multilamellar vesicles (MLVs) [10]. Their polar headgroup has a smaller diameter than the hydrocarbon chain region in the fluid phase. This results in a molecular shape of a truncated cone and an intrinsic propensity of PE bilayers to form surfaces with a negative curvature, leading to the formation of non-lamellar phases at elevated temperatures [11]. PGs, in contrast, are negatively charged at pH > 5 and therefore form unilamellar vesicles (ULVs) when the electrostatic repulsion is not screened by counter-ions in the aqueous solution [12,13]. Because of their cylindrical molecular shape, they prefer to form flat bilayers even at high temperatures. Besides pH, their thermotropic properties depend strongly on the ionic strength of the aqueous solution, lipid concentration and incubation time at low temperatures ([12], and references therein). For salt concentrations below 100 mM, the melting of the hydrocarbon chains occurs through the formation of an intermediate defect-rich phase [12,14]. In contrast, at salt concentrations above 100 mM, PGs display a sharp melting transition analogous to that observed in PCs [15]. Further similarities to PCs, in the case of high pH and ionic strength, are the tilting of the hydrocarbon chains with respect to bilayer plane [16], as well as the formation of subgel [17] and ripple phases [13].

Mixtures of PEs and PGs have to accommodate the different properties of the individual lipids. The thermodynamic mixing properties of disaturated PEs and PGs have been studied as a function of pH and acyl chain length at high (>100 mM) and low (<100 mM) ionic strength, respectively [18,19]. The largest effect was observed with respect to pH due to changes in PG headgroup protonation

state (PG has a pK_a value of ~3 [20,21]). However, PE/PG mixtures with equal chain length, i.e., di14PE/di14PG and di16PE/di16PG, showed very similar non-ideal mixing behavior irrespective of the electrolyte concentration [18,19].

The present work focuses on two aspects. The first is the dependence of the vesicular lamellarity on the lipid composition under physiologically relevant buffer conditions (20 mM Na-phosphate buffer, 130 mM NaCl, pH 7.4), i.e., at high ionic strength. Under these circumstances, the PG headgroups are completely deprotonated, but the electrostatic interactions between adjacent membranes are partially screened by the presence of counter ions. We find that mixtures of POPE and POPG form vesicles that consist of only very few bilayers, on the order of three to five, so-called oligolamellar vesicles (OLVs). Below the main phase transition temperature, T_m, the bilayers within the OLVs are positionally correlated and we observe Bragg reflections in the small angle X-ray diffraction patterns. The separation between the bilayers increases with PG content up to a molar concentration of $x_{POPG} = 0.5$ and remains constant up to $x_{POPG} = 0.9$, indicating a phase segregation. Interestingly, the average number of bilayers of the OLVs remains unaffected by the PG concentration. Above T_m the bilayers loose, at all PE/PG ratios, positional correlations and the scattered intensity corresponds to those of freely fluctuating, unbound, membranes.

The second focus of the present work is on the influence of the hydrocarbon chain composition on the phase behavior and in particular on the role of hydrocarbon chain unsaturation with respect to the thermodynamic mixing properties of the two lipid species. Here, we find that the unsaturated lipids POPE and POPG show, analogous to the disaturated species at the same pH conditions [18,19], a non-ideal mixing in all phases, irrespective of electrolyte concentration. The phase diagram exhibits, in agreement with the results for the bilayer separation, a miscibility gap at high PG concentration, which has again been found also for PE/PG of disaturated species [19]. The thermodynamic mixing properties are therefore a general feature of membranes composed of PE/PG that is dominated by the electrostatics of the headgroup but largely independent of the composition of the hydrocarbon chains. This is in good agreement with a recent theoretical prediction by May et al. [22].

2. Materials and methods

2.1. Lipids and chemicals

POPE and POPG were purchased from Avanti Polar Lipids, Inc., Alabaster, AL, USA (purity > 99%) as powder and used without further purification. Lipid stock solutions were prepared by dissolving weighted amounts of the respective lipid in chloroform containing 10 vol.% methanol

in a cold room at 4 °C and used immediately. Prior and after measurements, the purity and possible degradation of the phospholipids was checked by thin layer chromatography (TLC) using $CHCl_3/CH_3OH/NH_{3,conc.}$ (70/10/1) (v/v/v) as solvent.

2.2. Preparation of liposomes

Appropriate amounts of POPE and POPG were mixed from freshly prepared stock solutions, dried under a stream of nitrogen and subsequently placed in a vacuum chamber overnight to remove residual traces of the organic solvent. The dry lipid films were hydrated in buffer (double-distilled water containing 20 mM Na-phosphate, pH 7.4, 130 mM NaCl) by vigorous vortex-mixing at 45 °C combined with six freeze and thaw cycles using liquid nitrogen. The lipid concentration of the samples was 1 mg/ml for DSC and 50 mg/ml for X-ray diffraction measurements, respectively.

Samples with POPG molar fractions $x_{POPG} > 0.6$ exhibit a main phase transition temperature, T_m, or transition onset temperature, T_{on}, close to or below 0 °C. These samples were therefore prepared in buffer containing 50 vol.% ethyleneglycol. This lowers the freezing point of water, thus preventing the freezing of the buffer solution. Control DSC heating scans at $x_{POPG} = 0.3$, 0.5, and 0.6 in the presence and absence of the antifreeze gave very similar results for transition on and offset temperatures as well as phase transition temperature, while showing minor differences in transition enthalpy (data not shown). This finding is in agreement with earlier data demonstrating negligible effects of ethyleneglycol on dimyristoylphosphatidylcholine liposomes [23].

2.3. Differential scanning calorimetry

Calorimetric experiments were performed on a MicroCal VP-DSC high-sensitivity differential scanning calorimeter (MicroCal, Inc., Northampton, MA, USA) applying a heating scan rate of 30 °C/h. This scan rate was determined as the fastest and therefore optimal choice showing no scan rate dependent influence on T_{on} and T_{off} from a series of DSC experiments. All liposomal dispersions were degassed for 10 min prior to measurement. The on- and offset temperatures were determined by the tangent method as the intersection of the peak slopes with the baseline of the thermograms [24]. T_{on} and T_{off} are then corrected by the finite widths of the transitions of the pure components weighted with their mole fractions according to a method described earlier [25]. The phase transition temperature (T_m) is taken as the temperature of maximum heat capacity ($\Delta c_{p,max}$) and calorimetric enthalpies were calculated by integrating the peak areas, after baseline adjustment and normalization by the lipid concentration, using MicroCal's Origin software. The same software is also used to determine the transition half width $\Delta T_{1/2}$.

2.4. Simulation of the phase diagram

The applied simulation of the phase diagram is based on regular solution theory using non-ideality parameters for describing deviations from ideal mixing behavior [26] and has been described in detail before [26,27]. Negative non-ideality parameters (ρ_i) indicate the preference of pair formation of unlike molecules (A−B), whereas positive ones indicate the preferential formation of like pairs (A−A or B−B) [27]. In other words, a positive ρ reflects immiscibility between the lipids, resulting in a lateral phase separation and domain formation of lipids of the same type and in the same phase, whereas negative ρ values reflect a tendency to ordered, "chessboard" type mixing of the two lipids in the membrane plane.

Due to the fact that these non-ideality parameters are in most cases a function of the composition, a non-ideal, non-symmetric model is chosen. Within the framework of this model, the excess free energy $\Delta G^E = x(1−x)[\rho_1 + \rho_2(2x−1)]$, with x being the mole fraction and ρ_i the non-ideality parameters (ρ_1 describes the non-ideal mixing at $x = 0.5$ and ρ_2 accounts for the asymmetry term of the non-ideality).

The input parameters for the phase diagram simulation are the phase transition temperature, the phase transition enthalpy of the pure components, as well as the transition onset and offset temperatures for all lipid mixtures. From this, we obtain the solidus and liquidus curves, as well as two non-ideality parameters for the fluid (ρ_{f1} and ρ_{f2}) and for the gel phase (ρ_{g1} and ρ_{g2}). In order to increase reliability, the non-ideality parameters are usually combined as $\Delta\rho_1 = \rho_{f1} − \rho_{g1}$ and $\Delta\rho_2 = \rho_{f2} − \rho_{g2}$.

2.5. X-ray diffraction

X-ray diffraction patterns of samples with $x_{POPG} \leq 0.5$ were recorded in the small-(SAXS) and wide-angle (WAXS) regions using a SWAX camera [28] (Hecus X-ray Systems, Graz, Austria). The X-ray camera was mounted on a sealed-tube generator (Seifert, Ahrensburg, Germany) operating at 2 kW. SAXS diffraction patterns in the range 10^{-3} Å$^{-1} < q < 1$ Å^{-1} and WAXS diffraction patterns in the range 1.2 Å$^{-1} < q < 2.7$ Å^{-1} were recorded simultaneously using two linear, one-dimensional, position-sensitive detectors, where $q = 4\pi \sin\theta/\lambda$ is the scattering vector. CuK$_\alpha$ radiation ($\lambda = 1.542$ Å) was selected using a Ni filter in combination with a pulse height discriminator. Samples were filled in sealed 1 mm diameter quartz-glassed capillaries and kept in good thermal contact with a programmable Peltier unit, which allows temperature control in the range of 0 °C to 70 °C. Samples were equilibrated for 10 min at each temperature prior to measurement. The exposure time was set to 1000 s for the SAXS and 2000 s for the WAXS regime, respectively. Diffraction patterns were calibrated using silver behenate [29] for the small-angle regime and p-bromo-benzoic acid [30] for the wide-angle regime.

Samples with $x_{POPG} > 0.5$ were measured at the Austrian SAXS beamline at the Italian synchrotron radiation source Elettra [31]. Similar to the set-up in Graz, diffraction patterns were recorded with one-dimensional gas detectors [32] at the same time in the SAXS and WAXS regime in a comparable range of scattering vectors. The photon energy was set to 8 keV, which corresponds to a wavelength $\lambda = 1.5498$ Å. Sealed glass capillaries containing the liposomal dispersions were placed into an in-line micro-calorimeter, which permits the simultaneous performance of DSC and X-ray diffraction experiments [33]. This set-up also allows the recording of X-ray scattering data below 0 °C. DSC data obtained this way are qualitatively similar to that obtained with the MicroCal VP-DSC and are, therefore, not shown.

The X-ray diffraction data below the T_m was background corrected and analyzed in terms of a global model described previously [34,35] taking into account the different instrumental influences of the synchrotron and SWAX camera set-up. Briefly, the scattered intensity is described as

$$I(q) = \frac{S(q)|F(q)|^2}{q^2} + N_u \frac{|F(q)|^2}{q^2}, \qquad (1)$$

where $S(q)$ is the structure factor taking into account the nature of the crystalline lattice, $F(q)$ the form factor given by the Fourier transform of a Gaussian model for the electron density profile and N_u a scaling factor accounting for additional diffuse scattering from uncorrelated bilayers. We choose a paracrystalline structure factor [36], which includes the effect of bilayer stacking disorder, but neglects bending fluctuations, which can safely assumed to be absent below the T_m. From this analysis, we obtain the lamellar repeat distance, membrane thickness, bilayer separation and an estimate for the average number of bilayers within the vesicles.

2.6. Optical microscopy

The microscopy images were acquired using the Axiovert 135 inverted microscope (Zeiss, Germany) in phase contrast mode. The objective used was of magnification $40\times$. The sample was placed in a home-made glass chamber and temperature-controlled with a circulating water bath to within ± 0.1 °C. The sample was equilibrated at a given temperature for at least 5 min before taking a snapshot. Because vesicles were freely diffusing within the chamber, it is safe to assume that they were not sticking to the glass wall.

3. Results and discussion

Fig. 1 gives an overview of the DSC heating scans at all PE/PG ratios, while Table 1 summarizes the thermodynamic parameters. The results for pure POPE are in good agreement with previously published data [37]. In contrast, and to the best of our knowledge, no thermodynamic parameters
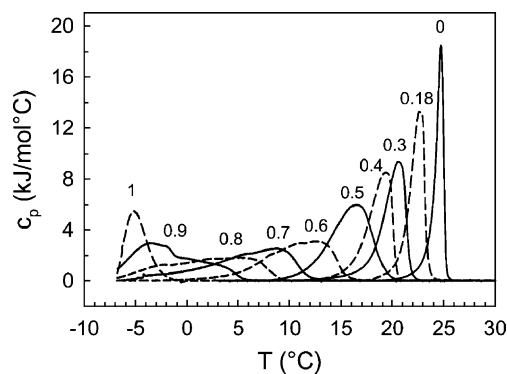

Fig. 1. DSC heating thermograms of POPE/POPG mixtures at various POPG concentrations (numbers adjacent to data give the molar fraction of POPG (x_{POPG}). Mixtures with $x_{POPG} \geq 0.6$ were hydrated in buffer containing 50% vol. ethylenglycol. For better graphical representation, thermograms of some samples have been omitted.

are available so far for pure POPG. Usually, it is assumed that the chain melting of PGs at pH > 5 and high ionic strength occurs in the same temperature range as their PC chain analogs. In the case of POPC, the T_m has been reported to lie between -5 and 0 °C [38]. We find a chain melting of POPG at $T_m = -5.3$ °C, which agrees with the above assumption.

Fig. 2 shows all on and offset temperatures deduced from the DSC scans, as well as the solidus and liquidus lines obtained by the simulation described above. Both liquidus and solidus curves, respectively, show a reasonable agreement between model and experimental data. The shape of the phase diagram clearly deviates from a "cigar" like shape known from ideal mixtures. This indicates a thermodynamically non-ideal miscibility of POPE and POPG. The difference of the non-ideality parameters is $\Delta\rho_1 = -700$ J/mol and $\Delta\rho_2 = +1600$ J/mol with $\rho_{g1} > \rho_{f1}$ and $\rho_{f2} > \rho_{g2}$. The second parameter ($\Delta\rho_2$) illustrates the strong asymmetry of the phase diagram, while phase diagrams with a "cigar" like shape have non-ideality parameters around zero [18,39]. The liquidus curve points to non-ideal mixing throughout the whole composition range. In contrast, the solidus line has a straight form for $x_{POPG} \sim 0.75 - 1.0$, indicating the presence of a miscibility gap, i.e., the formation of gel-like lipid domains with different PE/PG compositions.

X-ray diffraction experiments have been carried out in order to assign the phase and to determine the lamellar morphology of the mixtures. Fig. 3 shows the diffraction patterns for all PE/PG mixtures in the gel phase, including those of pure POPE and POPG. The SAXS patterns of pure POPE exhibit sharp Bragg reflections corresponding to a lamellar d-spacing of 62.2 ± 0.1 Å. Most prominent is the first order reflection. Higher orders are also present, but of low intensity, such that they cannot be seen on the linear intensity scale. The linear scale is better suited to demonstrate the sharpness of the Bragg peaks. It is well known that the central width of a Bragg peak is determined by the finite-size of the scattering domains [35,40]. The larger the domain

Table 1
Thermodynamic parameters of the L_β to L_α phase transition of POPE/POPG mixtures

x_{POPG}	T_m (°C)	ΔH_{cal} (kJ/mol)	T_{on} (°C)	T_{off} (°C)	$\Delta T_{1/2}$ (°C)	$\Delta c_{p, max}$ (kJ/mol °C)
0	24.7	20.5	24.7	24.7	0.8	18.0
0.05	24.5	23.0	22.2	24.9	1.5	11.7
0.10	23.7	27.2	21.7	23.9	1.6	14.2
0.13	23.4	28.4	22.1	23.8	1.6	15.0
0.15	23.1	26.7	22.1	23.9	1.2	18.4
0.18	22.7	24.2	21.5	23.2	1.5	13.4
0.30	20.6	25.5	17.4	21.4	2.3	9.2
0.40	19.4	24.2	14.3	19.9	2.5	8.4
0.50	15.4	29.3	10.1	16.5	4.5	5.8
0.60	12.6	23.8	3.1	13.8	7.4	2.9
0.70	8.7	23.0	−2.6	10.0	8.2	2.5
0.75	7.6	18.8	−5.5	8.5	8.7	2.1
0.80	4.8	19.6	−6.9	7.7	11.8	1.7
0.90	−3.7	21.7	−6.3	3.3	7.4	2.9
1	−5.3	20.5	−5.3	−5.3	2.7	5.4

size, the smaller the width of the Bragg peak. In the present case, the observed peak width is determined by the resolution of the camera which puts an upper limit of 1600 Å to the domain size that can be determined from the global data analysis [35]. This limit corresponds, at the observed lamellar repeat distances, to about 25 bilayers per scattering domain. Hence, the POPE vesicles consist of at least 25 bilayers and can therefore, in agreement with previous studies on POPE in pure water [10], be considered as MLVs. Further, apparently the presence of ions in the buffer has no influence on the lamellar aggregation form of pure POPE. WAXS data show a single peak at 1.461 Å^{-1} (Fig. 4) given by the in-plane packing of the hydrocarbon chains. The peak position corresponds to an average separation of the hydrocarbon chains of 4.3 Å and is characteristic of a hexagonal packing of the hydrocarbon chains in an all-*trans* conformation pointing perpendicular

Fig. 3. SAXS patterns of POPE/POPG mixtures in the L_β phase. Panel A shows data for $0 < x_{POPG} \leq 0.5$ recorded with the SWAX camera. Panel B gives the synchrotron data in the x_{POPG} range of 0.7 to 1. Solid lines give the global fits to the scattering data. Numbers adjacent to diffraction data give the respective x_{POPG} values. h denotes the lamellar diffraction order. Dashes indicate the position of the first order Bragg peak in panel A and the second order in panel B. Offsets have been added to shift the data vertically.

from the plane of the bilayer towards the bilayer center [41]. Hence, the correct phase assignment for pure POPE below the T_m is L_β.

In contrast to pure POPE, its phosphatidylglycerol analog, POPG, exhibits no Bragg peaks but solely diffuse scattering below the T_m (Fig. 3). The observed scattering is due to the Fourier transform of the electron density distribution within single, uncorrelated bilayers and is characteristic for ULVs. From the global fit to the diffraction pattern in the gel phase (Fig. 3), we find a head-to-headgroup distance of $d_{HH} = 45.6 \pm 0.2$ Å. This contrasts with the $d_{HH} = 48.4 \pm 0.2$ Å that we find for pure POPE. POPG forms ULVs under present conditions because of the negative charge of the lipids, which leads to a net electrostatic repulsion of the bilayers. This is a general observation for charged lipids and has been well documented both experimentally [42,43] and theoretically [44]. The hydrocarbon chain reflection is again symmetric with a slightly
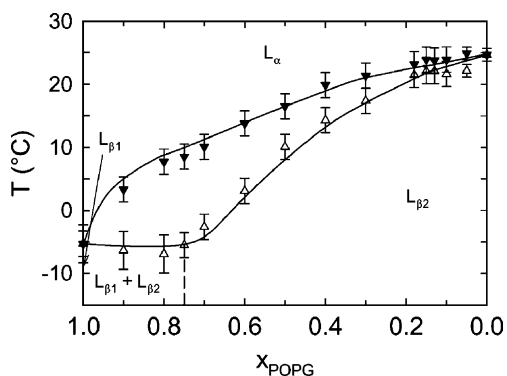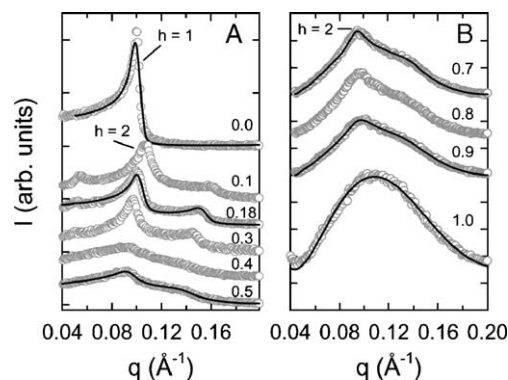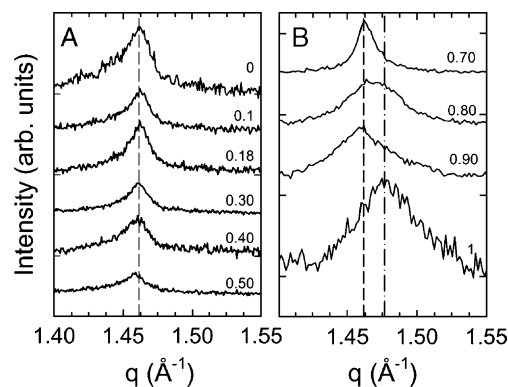

Fig. 2. Phase diagram for POPG/POPE mixtures as determined from the heat capacity functions. The coexistence lines (solidus and liquidus curve) are calculated using the four-parameter model for non-ideal, non-symmetric mixing as described in the Materials and methods section. The dashed line is a schematic representation of the coexistence line of this miscibility gap. ($\triangle$)s correspond to the experimental T_{on} and ($\blacktriangledown$)s to the T_{off} of the main phase transition. The assignment of the phases is deduced from WAXS data (see Fig. 4).

Fig. 4. WAXS patterns of POPE/POPG mixtures in the L_β phase. Panel A shows data for $0 < x_{POPG} \leq 0.5$ recorded with the SWAX camera. Panel B gives the synchrotron data in the x_{POPG} range of 0.7 to 1. Numbers adjacent to diffraction data give the respective x_{POPG} values. The dashed line indicates the position of the POPE hydrocarbon peak and the dashed-dotted line the one from pure POPG. Offsets have been added to shift the data vertically.

lower d of 4.26 Å (Fig. 4). Thus, also for POPG, the chains are packed on a 2D hexagonal lattice and are not tilted with respect to the membrane normal. In order to differentiate between the two gel phase packings, we will call the gel phase of pure POPE $L_{\beta 2}$ and that of pure POPG $L_{\beta 1}$ (see also Fig. 2).

The addition of POPG to POPE has a remarkable effect on the lamellar periodicity: it jumps from 62.2 Å in the case of pure POPE to 113 Å at the lowest POPG concentration measured (Fig. 3). The increase in the lamellar repeat distance is accompanied by a significant increase in the peak width. Interestingly, the second order Bragg reflection now exhibits a higher intensity than the first order reflection. This is due to the "weighting" of the peaks by the absolute square of the form factor $F(q)$ (Eq. 1). $|F(q)|^2$ is small at the position of the first order peak and has a maximum near the second order peak. This attenuates the first order and enhances the second order reflection. The reason for the large increase in d is the negative surface charge induced by POPG, which leads to a strong electrostatic repulsion between adjacent layers and hence to an increase of the bilayer separation [45]. Because of the counter ions present in the buffer, however, the repulsion is partially screened. Thus, the system does not unbind completely to form ULVs, but rather attains a finite separation of the bilayers. The lamellar repeat distance increases further with the addition of POPG as evidenced by the shift of the Bragg peaks to lower scattering angles (Fig. 3) and is shown for all PG concentrations in Fig. 5. The first order reflection vanishes at $x_{POPG} = 0.5$. Higher POPG concentrations exhibit only the second order peak and a weak shoulder from the third order. Our global fit of the X-ray patterns gives a d_{HH} value of about 48 Å for all mixtures. Besides showing that the membrane thickness is dominated by POPE, this finding demonstrates that the increase of d is due to an increase of the bilayer separation resulting from a stronger electrostatic repulsion as more and more PG is included in the membrane.

Interestingly, the evolution of the d spacing saturates and attains a value of 132 Å at x_{POPG} around 0.5. Since the electrostatic interactions are dominated by the surface
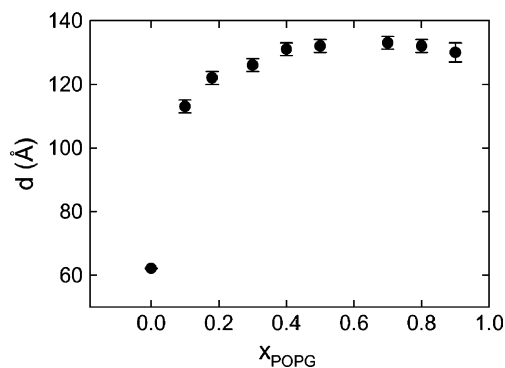
charge density, this finding indicates that it gets more and more difficult to increase the charges within the membrane until finally no more PG can be incorporated for $x_{POPG} > 0.5$. This is a signature of phase segregation and agrees, besides a slightly lower x_{POPG} value for the border line, well with our thermodynamic results (Fig. 2). The excess of PG that cannot be included into the PE/PG membranes at higher PG content will most likely form pure POPG ULVs that coexist with vesicles composed of POPE and POPG.

There is another interesting detail regarding the lamellarity of the PE/PG mixtures: While the Bragg peaks shift to lower angles and decrease in intensity, their central width is much broader than in the case of pure POPE but stays essentially constant with PG concentration (Fig. 3). In the case of POPE, we concluded that the width, relating to the average number of lamellae per scattering domain, is resolution limited. This is not the case for the PE/PG mixtures. Here, our global X-ray data analysis yields that the number of bilayers is on the order of three to five and shows no trend with respect to the PG concentration. This indicates the formation of oligolamellar vesicles (OLVs), whose number of bilayers does not depend on PG content. Within the miscibility gap the OLVs coexist with ULVs composed of pure POPG, as described above.

While the addition of POPG to POPE had dramatic effects on the bilayer morphology the hydrocarbon chain packing shows little changes due to the presence of PG (Fig. 4). In the x_{POPG} range of 0 to 0.5, all hydrocarbon peaks are symmetric and centered at $2\pi/4.3$ Å^{-1}. Similar to the supramolecular structure, the hydrocarbon packing is therefore also dominated by the POPE chains. Hence, we denote the gel phase within this PG concentration regime also as $L_{\beta 2}$ (Fig. 2). A further increase of POPG up to $x_{POPG} = 0.9$ leads to a progressive broadening of the hydrocarbon chain reflection and renders the peak shape asymmetric (Fig. 4B). The tailing occurs towards higher scattering angles and coincides with the position of the POPG wide angle peak at $2\pi/4.26$ Å^{-1}. Apparently, the asymmetry is due to an overlap of the POPE/POPG ($L_{\beta 2}$) chain reflection with that of POPG ($L_{\beta 1}$). Hence, the scattering data indicate a demixing of POPE and POPG as also manifest from our results above.

We now turn to the structure of the POPE/POPG mixtures above the T_m. Here, all wide-angle diffraction patterns show a broad peak centered at around $2\pi/4.5$ Å^{-1} (data not shown), demonstrating that the system is in the L_α phase. The SAXS patterns are shown in Fig. 6. Remarkably, with the exception of the pure POPE, all samples exhibit pure diffuse scattering. This is in contrast to the gel phase, where Bragg peaks were observed up to POPG concentrations of 0.9 (Fig. 3). Apparently, the system transforms in the x_{POPG} range of 0.1–0.9 from a state where the bilayers are positionally correlated (bound state) below the T_m to a state where there are no positional correlations between adjacent bilayers (unbound state) above the T_m. This is called a thermal unbinding transition and has been
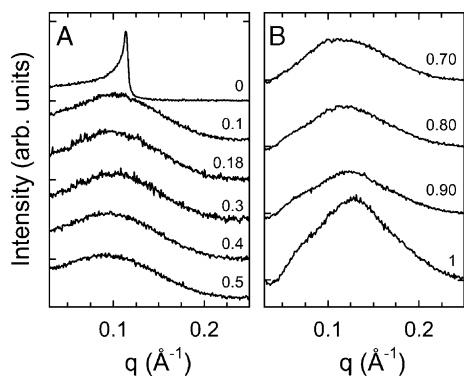

Fig. 5. Lamellar repeat distance of POPE as a function of POPG content determined from the global SAXS data analysis.

Fig. 6. SAXS of the POPE/POPG mixtures in the L_α phase at 30 °C. Numbers adjacent to diffraction data give the molar fraction of POPG. Data recorded in the x_{POPG} range from 0 to 0.5 with the SWAX camera is shown in panel A. Panel B gives the SAXS data in the x_{POPG} range of 0.7 to 1 recorded at the SAXS beamline at ELETTRA, Trieste.

Fig. 7. Phase contrast optical microscopy images of a single OLV composed of POPE/POPG at $x_{POPG}=0.18$ as a function of temperature. The vesicle shows a well defined border below T_m ((A), $T=18$ °C), which becomes fussy in the unbound state above T_m ((B), $T=24$ °C) due to enhanced fluctuations. The bilayer arrangement is schematically shown in the insets.

described theoretically [46,47] and experimentally for the present system [45].

Briefly, bilayers are positionally correlated in the gel phase via their attractive van der Waals and the repulsive electrostatic interactions. However, the correlation is weak, which is also evidenced by the large separation between adjacent bilayers and large width of the Bragg peaks. Thus, compared to non-charged lipid membranes, the present system can be easily transformed into an unbound state. Now, as the system is transformed into the fluid phase at the T_m, the bending rigidity of the bilayers drops by about one order of magnitude [45,48]. This causes a significant increase of bilayer undulations, leading to the well-known Helfrich repulsion [49], which, in the present case, is strong enough to destabilize the membrane stack. The unbinding transition is fully reversible and the system returns into its bound state when cooled back below T_m [45].

With respect to the unbinding transition, there remains one open question that we did not address in our previous paper [45], but which is of interest to the present study: What is the lamellar aggregation form in the unbound state? Are the vesicles unilamellar, or do they remain oligolamellar but positionally uncorrelated? Both cases, ULVs and uncorrelated bilayers within a OLV, respectively, yield similar, pure diffuse SAXS patterns. There might be some change in intensity at very low scattering angles, because of a possible change in vesicle size in going from OLV to ULV. However, due to the large vesicle size (~10 μm; see Fig. 7), such changes cannot be resolved with the present experimental set-up. The most direct answer to the above question can be obtained from optical phase contrast microscopy. Fig. 7 shows the results of such an experiment. At low temperatures, the vesicle has an almost spherical shape and shows a well-defined border line (Fig. 7A). The contrast from the membrane indicates that the vesicles consist of a few bilayers in agreement with our global X-ray data analysis. However, when the temperature is increased above the T_m, the border line becomes very fuzzy (Fig. 7B). This is due to the loss of positional correlations between the
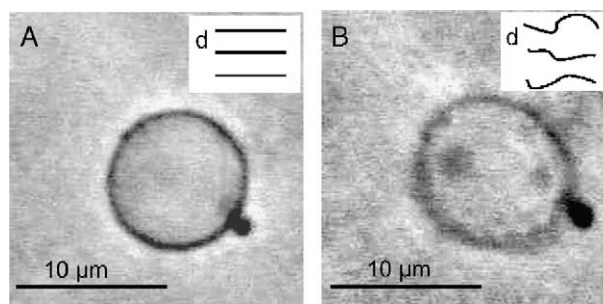
bilayers. More important, the vesicle remains intact and does not break up into ULVs. Hence, the unbound state is characterized by OLVs comprised of freely fluctuating and hence uncorrelated bilayers. Fig. 7 also shows that the inner core of the vesicle is rather large. This is important to place no restrictions on the unbinding by imposing a tension within the vesicle through stress, as would be the case for vesicles with a small inner core (Lipowsky, R., personal communication).

4. Summary and conclusion

We have determined the lamellar morphology and mixing properties of POPE/POPG mixtures under physiological relevant conditions (20 mM Na-phosphate buffer, 130 mM NaCl, pH 7.4). Our findings are summarized in the schematic representation shown in Fig. 8. POPE/POPG exhibits non-ideal mixing properties in the fluid phase and
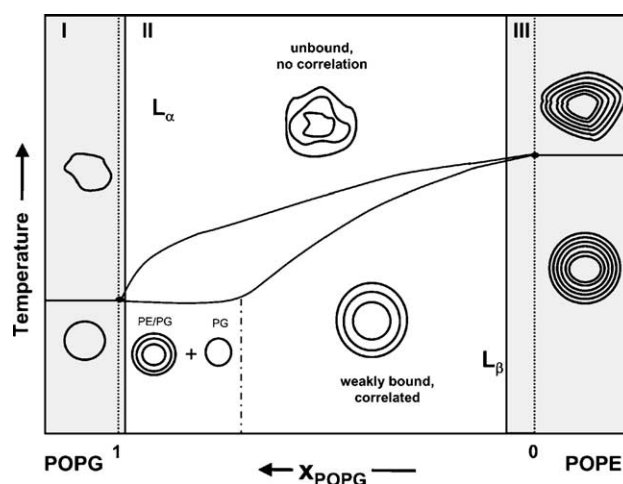

Fig. 8. Schematic representation of the vesicle morphology as a function of POPE/POPG composition and phase state. The phase diagram exhibits a miscibility gap at $x_{POPG}>0.70$ indicated by the straight solidus line in this composition range. Panel I corresponds to the existence range of unilamellar vesicles, panel II to oligolamellar vesicles and panel III to multilamellar vesicles.

in the gel phase as demonstrated by the strong asymmetry of the liquidus/solidus line. The morphology of the system changes from MLVs for pure POPE to OLVs with a roughly constant number of three to five bilayers for POPE/POPG mixtures and finally exhibits ULVs for pure POPG. The bilayers within the OLVs are positionally correlated within the gel phase but become uncorrelated upon entering the L_α phase, triggered by a drop in the bilayer bending rigidity at the T_m [45]. However, while positional correlations are lost, the vesicles as a whole remain intact as evidenced by phase contrast microscopy (Fig. 7).

Another important feature of the binary mixture is the existence of a miscibility gap at PG concentrations above 70 mol% that we observe independently from DSC, SAXS and WAXS experiments. This region of phase segregation appears to be a general feature of PE/PG mixtures, as it has been also observed for di14PE/di14PG and di16PE/di16PG at high [18] and for di16PE/di16PG at low ionic strength [19], respectively. Additional evidence for this notion has been reported from fluorescence studies on model [50], as well as on *E. coli* and *B. subtilis* membranes [51]. These findings are further in remarkable agreement with mean field calculations based on the Poisson–Boltzmann theory, which predict a critical concentration of charged lipids of 0.63 above which demixing is expected [22]. Hence, the two-dimensional organization in PE/PG membranes appears to be dominated by head-group interactions and to be largely independent on hydrocarbon chain length or degree of saturation. Formation of lipid domains with different compositions is consequently unavoidable in mixtures with excess of the negatively charged component.

Acknowledgements

References

[1] K. Lohner, R.M. Epand, Membrane interactions of haemolytic and antibacterial peptides, in: C.A. Bush (Ed.), Advances in Biophysical Chemistry, JAI Press Inc, Greenwhich, 1997, pp. 53–66.

[2] K. Lohner, E.J. Prenner, Differential scanning calorimetry and X-ray diffraction studies of the specificity of the interaction of antimicrobial peptides with membrane-mimetic systems, Biochim. Biophys. Acta 1462 (1999) 141–156.

[3] K. Lohner, The role of membrane lipid composition in cell targeting of antimicrobial peptides, in: K. Lohner (Ed.), Development of Novel Antimicrobial Agents: Emerging Strategies, Horizon Scientific Press, Norfolk, 2001, pp. 149–165.

[4] K. Lohner, S.E. Blondelle, Molecular mechanisms of membrane perturbation by antimicrobial peptides and the use of biophysical studies in the design of novel peptide antibiotics, Comb. Chem. High Throughput Screen. 8 (2005) 241–256.

[5] M.A. Yorek, Biological distribution, in: G. Cevc (Ed.), Phospholipid handbook, Marcel Dekker, Inc., New York, 1993.

[6] J.E. Rothman, J. Lenard, Membrane asymmetry, Science 195 (1977) 743–753.

[7] M. O'Leary, S.G. Wilkinson, Gram-positive bacteria, in: C. Ratledge (Ed.), Microbial Lipids, Academic Press, London, 1988, pp. 117–201.

[8] S.G. Wilkinson, Gram-negative bacteria, in: C. Ratledge, S.G. Wilkinson (Eds.), Microbial Lipids, Academic Press, London, 1988, pp. 299–488.

[9] P. Laggner, K. Lohner, Liposome phase systems as membrane activity sensors for peptides, in: J. Katsaras, T. Gutberlet (Eds.), Lipid bilayers, Structure and interactions, Springer, Berlin, 2000, pp. 233–264.

[10] M. Rappolt, P. Laggner, G. Pabst, Structure and elasticity of phospholipid bilayers in the L_α phase: a comparison of phosphatidylcholine and phosphatidylethanolamine membranes, in: S.G. Pandalai (Ed.), Recent Research Developments in Biophysics, Transworld Research Network, Kerala, 2004, pp. 363–394.

[11] J.M. Seddon, R.H. Templer, Polymorphism of lipid water systems, in: R. Lipowsky, E. Sackmann (Eds.), Structure and dynamics of membranes, North-Holland, Amsterdam, 1995, pp. 97–160.

[12] K.A. Riske, L.Q. Amaral, H.G. Döbereiner, M.T. Lamy, Mesoscopic structure in the chain-melting regime of anionic phospholipid vesicles: DMPG, Biophys. J. 86 (2004) 3722–3733.

[13] G. Degovics, A. Latal, K. Lohner, X-ray studies on aqueous dispersions of dipalmitoylphosphatidylglycerol in the presence of salt, J. Appl. Crystallogr. 33 (2000) 544–547.

[14] M.F. Schneider, D. Marsh, W. Jahn, B. Kloesgen, T. Heimburg, Network formation of lipid membranes: triggering structural transitions by chain melting, Proc. Natl. Acad. Sci. U. S. A. 96 (1999) 14312–14317.

[15] Y.P. Zhang, R.N. Lewis, R.N. McElhaney, Calorimetric and spectroscopic studies of the thermotropic phase behavior of the n-saturated 1,2-diacylphosphatidylglycerols, Biophys. J. 72 (1997) 779–793.

[16] A. Watts, K. Harlos, D. Marsh, Charge-induced tilt in ordered-phase phosphatidylglycerol bilayers evidence from X-ray diffraction, Biochim. Biophys. Acta 645 (1981) 91–96.

[17] A.E. Blaurock, T.J. McIntosh, Structure of the crystalline bilayer in the subgel phase of dipalmitoylphosphatidylglycerol, Biochemistry 25 (1986) 299–305.

[18] P. Garidel, A. Blume, Miscibility of phosphatidylethanolamine–phosphatidylglycerol mixtures as a function of pH and acyl chain length, Eur. Biophys. J. 28 (2000) 629–638.

[19] K. Lohner, A. Latal, G. Degovics, P. Garidel, Packing characteristics of a model system mimicking cytoplasmic bacterial membranes, Chem. Phys. Lipids 111 (2001) 177–192.

[20] A. Watts, K. Harlos, W. Maschke, D. Marsh, Control of the structure and fluidity of phosphatidylglycerol bilayers by pH titration, Biochim. Biophys. Acta 510 (1978) 63–74.

[21] G. Cevc, Membrane electrostatics, Biochim. Biophys. Acta 1031 (1990) 311–382.

[22] S. May, D. Harries, A. Ben Shaul, Macroion-induced compositional instability of binary fluid membranes, Phys. Rev. Lett. 89 (2002) 268102.

[23] C.H. Fabrie, B. de Kruijff, J. de Gier, Protection by sugars against phase transition-induced leak in hydrated dimyristoylphosphatidylcholine liposomes, Biochim. Biophys. Acta 1024 (1990) 380–384.

[24] P. Garidel, C. Johann, and A. Blume, The calculation of heat capacity curves and phase diagrams based on regular solution theory, J. Thermal Analysis and Calorimetry (in press).

[25] S. Mabrey, J.M. Sturtevant, Investigation of phase transition of lipids

and lipid mixtures by high sensitivity differential scanning calorimetry, Proc. Natl. Acad. Sci. U. S. A. 73 (1976) 3862–3866.

[26] C. Johann, P. Garidel, L. Mennicke, A. Blume, New approaches to the simulation of heat-capacity curves and phase diagrams of pseudobinary phospholipid mixtures, Biophys. J. 71 (1996) 3215–3228.

[27] P. Garidel, C. Johann, A. Blume, Thermodynamics of lipid organization and domain formation in phospholipid bilayers, J. Liposome Res. 10 (2000) 131–158.

[28] P. Laggner, H. Mio, SWAX—A dual-detector camera for simultaneous small- and wide-angle X-ray diffraction in polymer and liquid crystal research, Nucl. Instrum. Methods Phys. Res., A 323 (1992) 86–90.

[29] T.C. Huang, H. Toraya, T.N. Blanton, Y. Wu, X-ray powder diffraction analysis of silver behenate, a possible low-angle diffraction standard, J. Appl. Crystallogr. 26 (1993) 180–184.

[30] K. Ohkura, S. Kashino, M. Haisa, The crystal and molecular structure of p-bromobenzoic acid, Bull. Chem. Soc. Jpn. 45 (1972) 2651–2652.

[31] H. Amenitsch, M. Rappolt, M. Kriechbaum, H. Mio, P. Laggner, S. Bernstorff, First performance assessment of the small-angle X-ray scattering beamline at ELETTRA, J. Synchrotron Radiat. 5 (1998) 506–508.

[32] A.M. Petrascu, M.H.J. Koch, A. Gabriel, A beginners' guide to gas-filled proportional detectors with delay line readout, J. Macromol. Sci., B 37 (1998) 463–483.

[33] G. Keller, F. Lavigne, L. Forte, K. Andrieux, M. Dahim, C. Loisel, M. Ollivon, C. Bourgaux, P. Lesieur, DSC and X-ray diffraction coupling—Specifications and applications, J. Therm. Anal. Calorim. 51 (1998) 783–791.

[34] G. Pabst, M. Rappolt, H. Amenitsch, P. Laggner, Structural information from multilamellar liposomes at full hydration: full q-range fitting with high quality X-ray data, Phys. Rev., E 62 (2000) 4000–4009.

[35] G. Pabst, R. Koschuch, B. Pozo-Navas, M. Rappolt, K. Lohner, P. Laggner, Structural analysis of weakly ordered membrane stacks, J. Appl. Crystallogr. 63 (2003) 1378–1388.

[36] A. Guiner, X-ray diffraction, Freeman, San Francisco, 1963.

[37] R. Koynova, M. Caffrey, Phases and phase transitions of the hydrated phosphatidylethanolamines, Chem. Phys. Lipids 69 (1994) 1–34.

[38] R. Koynova, M. Caffrey, Phases and phase transitions of the phosphatidylcholines, Biochim. Biophys. Acta 1376 (1998) 91–145.

[39] P. Garidel, C. Johann, L. Mennicke, A. Blume, The mixing behavior of pseudobinary phosphatidylcholine–phosphatidylglycerol mixtures as a function of pH and acyl chain length, Eur. Biophys. J. 26 (1997) 447–459.

[40] D. Sherwood, Crystals, X-Rays and Proteins, Longmann, London, 1976.

[41] A. Tardieu, V. Luzzati, F.C. Reman, Structure and polymorphism of the hydrocarbon chains of lipids: a study of lecithin–water phases, J. Mol. Biol. 75 (1973) 711–733.

[42] H. Hauser, Some aspects of the phase behaviour of charged lipids, Biochim. Biophys. Acta 772 (1984) 37–50.

[43] B. Deme, M. Dubois, T. Gulik-Krzywicki, T. Zemb, Giant collective fluctuations of charged membranes at the lamellar-to-vesicle unbinding transition: 1. Characterization of a new lipid morphology by SANS, SAXS, and electron microscopy, Langmuir 18 (2002) 997–1004.

[44] S. Leibler, R. Lipowsky, Complete unbinding and quasi-long-range order in lamellar phases, Phys. Rev., B 35 (1987) 7004–7009.

[45] B. Pozo-Navas, V.A. Raghunathan, J. Katsaras, M. Rappolt, K. Lohner, G. Pabst, Discontinuous unbinding of lipid multibilayers, Phys. Rev. Lett. 91 (2003) 028101.

[46] R. Lipowsky, S. Leibler, Unbinding transitions of interacting membranes, Phys. Rev. Lett. 56 (1986) 2541–2544.

[47] R. Lipowsky, From bunches of membranes to bundles of strings, Z. Phys., B Condens. Matter 97 (1995) 193–203.

[48] R. Dimova, B. Pouligny, C. Dietrich, Pretransitional effects in dimyristoylphosphatidylcholine vesicle membranes: optical dynamometry study, Biophys. J. 79 (2000) 340–356.

[49] W. Helfrich, Steric interaction of fluid membranes in multilayer systems, Z. Naturforsch. 33a (1978) 305–315.

[50] M. Uragami, T. Dewa, M. Inagaki, R.A. Hendel, S.L. Regen, Influence of head group mismatch on the miscibility of phospholipids in the physiologically-relevant fluid phase: a nearest-neighbour recognition analysis, J. Am. Chem. Soc. 119 (1997) 3797–3801.

[51] S. Vanounou, A.H. Parola, I. Fishov, Phosphatidylethanolamine and phosphatidylglycerol are segregated into different domains in bacterial membrane. A study with pyrene-labelled phospholipids, Mol. Microbiol. 49 (2003) 1067–1079.